

Proximity of current and vortex structures: effects on collisionless plasma heating

Tulasi N Parashar and William H Matthaeus

Bartol Research Institute, Department of Physics and Astronomy, University of Delaware, Newark, DE

Intermittency of heating in weakly collisional plasma turbulence is an active subject of research, with significant potential impact on understanding of the solar wind, solar corona and astrophysical plasmas. Recent studies suggest a role of vorticity in plasma heating. In magnetohydrodynamics small scale vorticity is generated near current sheets and this effect persists in kinetic plasma, as demonstrated here with hybrid and fully kinetic Particle-In-Cell (PIC) simulations. Furthermore, vorticity enhances local kinetic effects, with a generalized resonance condition selecting sign-dependent enhancements or reductions of proton heating and thermal anisotropy. In such plasmas heating is correlated with vorticity and current density, but more strongly with vorticity. These results help explain several prior results that find kinetic effects and energization near to, but not centered on, current sheets. Evidently intermittency in kinetic plasma involves multiple physical quantities, and the associated coherent structures and nonthermal effects are closely related.

I. INTRODUCTION

Weakly collisional plasmas in planetary magnetospheres [e.g. 1–3], stellar coronae [e.g. 4], solar and stellar winds [e.g. 5], black hole accretion disks [e.g. 6], galactic cooling flows [e.g. 7], and elsewhere, are observed [e.g. 2, 3, 8–10] or believed to be [e.g. 11, 12] in a turbulent state. These systems are typically more heated than what is expected from simplistic considerations [e.g. 13–16], a property consistent with turbulent cascade and dissipation. In these plasmas the conversion of larger fluid scale energy into thermal degrees of freedom must be accomplished by particle interactions with electromagnetic fields, leading ultimately to thermalization by collective effects or infrequent collisions [e.g. 17–19]. Understanding how collisionless processes lead to dissipation is an active research topic that is traditionally studied using linear Vlasov theory. A recent emphasis has been the study of intermittent, or spatially nonuniform, processes that occur in non-volume filling coherent structures, in analogy to intermittency properties in hydrodynamics. A specific focus of this work has been on electric current structures such as current filaments or current sheets. Intense kinetic activity, including temperature anisotropy, is found *near* current enhancements (sheets), but not necessarily centered on them [20–22]. Studies have also identified plasma flow vorticity and shear as important elements in heating and generation of kinetic effects [23–26]. Here we show that kinetic plasma generates vorticity structures, typically very close to current sheets or filaments. We will demonstrate that protons are preferentially heated in one sign of vorticity, and cooled in the other, confirming that the sign of $\omega \cdot \mathbf{B}$ controls this effect [23, 25]. This provides a unified interpretation of a number of recent results in the theory and simulation of kinetic plasma turbulence.

II. BACKGROUND

Various processes may contribute to the collisionless transfer of energy from fields into particles, e.g., wave-particle interactions [e.g. 19, 27] [28], heating at intermittent structures [e.g. 29–32], stochastic orbits [33], stochastic energization by electromagnetic fields at kinetic scales [e.g. 34, 35]. While it is not clear whether a single process is dominant under varying conditions (e.g. plasma β , Mach number, Alfvén ratio, etc.), a broader question is whether heating is mainly due to distributed homogeneous processes depending on average plasma properties (e.g., from linear Vlasov theory), or if the main contributors are inherently inhomogeneous localized processes, depending on gradients and intermittency of the turbulence.

Recent years have seen increasing evidence for intermittent heating, gathered from observations [e.g. 31, 36–38] as well as several types of numerical simulations [e.g. 20–22, 29, 30, 32, 39–41]. Efforts to *quantify* the nature of intermittency have also been made using MHD as well as kinetic simulations [e.g. 42, 43]. Most of these studies concentrate on coherent magnetic structures such as current sheets, reconnection sites, or “PVI” events [44]. However, some studies have also examined the role of structure in the (proton) velocity field. Studies have examined heating of protons in velocity shears [24], and the relation of enhanced heating to vorticity [26]. Hybrid simulations suggest [45] that the kinetic heating of protons might be a “viscous like” process instead of a magnetic process. This is not be unexpected since several types of coherent structures should emerge in turbulence and kinetic effects may appear in association with any, or all, of them, as can be readily demonstrated in solar wind observations [22].

Here we focus on vorticity, and show that vorticity structures appearing in kinetic plasma turbulence (in conditions roughly resembling the corona or solar wind) are intimately related to local current density enhancements. This effect that can be understood purely in terms of MHD processes [e.g. 46]. Plasma vortex struc-

tures are generated very close to current structures, typically taking on a quadrupolar configuration, and leading to plasma heating and generation of anisotropies in temperatures and pressure. Examining this effect in detail will lead to better understanding of dynamical activity near current sheets [20, 21, 41] including the involvement of vorticity in kinetic dissipation [24–26].

III. KINETIC SIMULATIONS

We employ two types of kinetic codes, hybrid particle-in-cell (PIC) and full PIC simulations. Both types make use of the P3D family of codes [47], in hybrid PIC [e.g. 30] mode, and fully kinetic PIC mode [e.g. 48]. All simulations discussed here are performed in the 2.5D geometry (2 dimensional grid and all three components of field vectors). The hybrid simulation has $L_x = L_y = 204.8d_i$ (where $d_i = c/\omega_{pi}$ is the ion inertial length, with c the speed of light and ω_{pi} the proton plasma frequency), $N_x = N_y = 2048$, 200 particles per cell, $\beta_i = 1.0$, cold isothermal electrons with $m_e/m_i = 1/25$. The simulation is initialized with energy only in wavevectors \mathbf{k} that have $|\mathbf{k}| = 3, 4, 5$. v and b fluctuations are chosen with a specified initial spectral shape, gaussian random phases, and only in essentially incompressible modes of the system. This simulation was also used in a recent study of variance anisotropy in kinetic plasmas [49]. The first full PIC simulation has $L_x = L_y = 20.48d_i$, $N_x = N_y = 1024$, 200 particles per cell, $\beta_i = \beta_e = 0.08$, $m_e/m_i = 1/25$. The initial condition is Orszag-Tang vortex (OTV) [e.g. 45, 50–52]. This simulation was performed for a recent study of transition from kinetic to MHD like behavior [53]. The final PIC simulation (Turb812) has $L_x = L_y = 25.6d_i$, $N_x = N_y = 2048$, 400 particles per cell, $\beta_i = \beta_e = 0.25$, $m_e/m_i = 1/25$. The latter initial condition is MHD like, and more “turbulent”, with v and b fluctuations excited in a band of wave-vectors with $2 \leq |k| \leq 4$ with a specified initial spectrum. This simulation was done as part of a recent study that discussed the relation of time scales at proton gyroscale and their relation to relative proton-electron heating [54]. Particle in cell codes have an inherent noise associated with them due to finite number of particles per cell. While performing these simulations, the two most important numerical criteria that we paid attention to were: i) excellent conservation of total energy (less than a few percent of change in any fluctuation energy) and, ii) the particle noise in the spectrum was significant only at scales much smaller than the scales of interest (Debye length λ_d for PIC and d_i for hybrid PIC). On this basis, the modest number of particles employed here was considered adequate. As an additional measure, we employed filtering [e.g. 40] to remove particle noise at grid scales prior to computing gradients (e.g. vorticity).

IV. VORTEX QUADRUPOLE GENERATION

The most commonly discussed coherent structures in plasma physics are current sheets and reconnection sites. However, these current concentrations are also locations of strong vorticity generation [e.g. 46]. This phenomenon, often overlooked in reconnection studies, may be completely understood in terms of two dimensional MHD, which we briefly review here.

The relevant equations of motion for two dimensional (2D) incompressible MHD can be written as [e.g. 55, 56]:

$$\frac{\partial \omega}{\partial t} + \mathbf{v} \cdot \nabla \omega = \mathbf{b} \cdot \nabla j_z + \nu \nabla^2 \omega \quad (1)$$

$$\frac{\partial a}{\partial t} + \mathbf{v} \cdot \nabla a = \mu \nabla^2 a \quad (2)$$

in terms of the z -component of vorticity $\omega = (\nabla \times \mathbf{v})_z$ and the magnetic potential $a(\mathbf{x}, t)$, where the fluctuating magnetic field is $\mathbf{b} = \nabla \times a(\mathbf{x}, t)\hat{z}$. The terms involving resistivity μ and viscosity ν are dissipative and become important at small scales. Although highly simplified, these contain the basic physics that establishes sites of magnetic reconnection, as in for example the well-known Sweet Parker model [57].

An important feature of the vorticity equation (1) is that when $\mathbf{b} \cdot \nabla j_z = 0$, Kelvin’s theorem applies and vorticity cannot be generated in the interior of the magnetofluid. However the term $\mathbf{b} \cdot \nabla j_z$, the curl of the Lorentz force, can generate vorticity, just as sheared velocity fields can stretch magnetic field lines and amplify the mean square current density. Taken together these two effects are responsible for amplification of gradients and the enhancement of dissipation that drive important relaxation processes in MHD [58–60].

Figure (1) provides a simple demonstration that vorticity generation is also operative in a kinetic plasma. The Figure shows the change in magnetic enstrophy (mean square electric current density $\Omega_b = \langle |J|^2 \rangle$) and the enstrophy (mean square vorticity $\Omega_v = \langle |\omega|^2 \rangle$) measured relative to their respective initial values for the hybrid run. Both Ω_b and Ω_v increase until a maximum value is reached after one or two nonlinear times. This behavior is familiar from MHD turbulence simulations that begin from band limited initial conditions (e.g., [59, 60]), the peak time being called in that case “the peak of dissipation”. Note that prior to the peak time, the mean square current increases somewhat more rapidly than the enstrophy. This behavior is common to all the kinetic turbulence simulations of this type, and also in MHD turbulence simulations with band limited initial data and fairly large and approximately equal Reynolds and magnetic Reynolds numbers. In both MHD and the kinetic case, this effect is indicative of the vorticity generation that is secondary to current sheet formation.

To further discuss vorticity generation, consider a purely 2D, or nearly 2D, geometry, and consider two oppositely directed flux tubes that encounter each other,

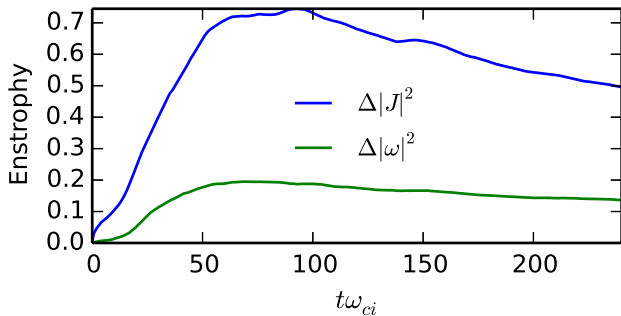
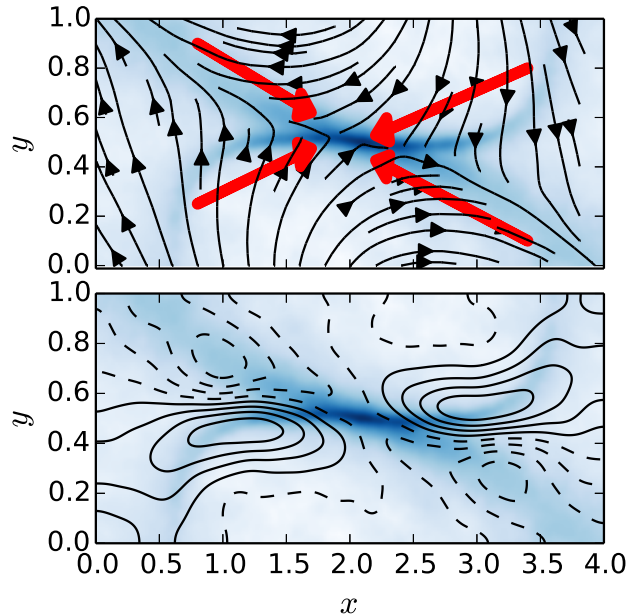


FIG. 1: Current grows before vorticity.

generating a current enhancement (say, in the positive z -direction) with a single maximum centered on the origin in the x - y plane, reminiscent of typical 2D reconnection geometry. Then ∇j_z is directed towards the origin in all four quadrants. The main magnetic field of the tubes is such that $b_x < 0$ for $y > 0$ and $b_x > 0$ for $y < 0$ (and we neglect the axial z -component of magnetic field for this demonstration.) One recognizes immediately [46] that the generation term $\mathbf{b} \cdot \nabla j_z$ is positive in the first and fourth quadrants, and negative in the second and fourth quadrants. That is a standard scenario of flux tube interactions giving rise to a current enhancement (filament or sheet). Once the current enhancement is formed, will also generate a vorticity quadrupole structure as shown in Figure IV.

It is noteworthy that the vorticity structures produced in this way necessarily form on the flanks of strong current enhancements. Moreover, the thickness of vortex structures produced in this way should be comparable to the thickness of the current sheet that drives them, in this case a few d_i . The similarity of vortex and current sheet thicknesses has been noted for example in the low beta weakly three dimensional Reduced MHD description of turbulence [61]. Furthermore qualitative evidence for this can be seen in fully kinetic PIC simulations [41] that electron vorticity structures as well as current structures extend down to electron scales, although correlations were not computed in that study.

The generation of vortex quadrupoles is a purely magnetohydrodynamic phenomenon that does not require any higher order effects like compressibility, Hall physics or any other kinetic effects. Therefore it is not entirely surprising that we can readily demonstrate that vortex quadrupole formation also occurs near current sheets in kinetic plasma simulation. For this we refer to the first two panels on the left side of each row in Figure (2). The top row shows an early time snapshot of the relatively ordered Orszag-Tang initial condition [50, 52], here simulated with a PIC code. The dynamics results immediately in several orderly current filaments, for example, the one that is found in the center of the simulation (first column, first row). One immediately sees clean vortex



Central current sheet from PIC OTV simulation (rotated by 30 degrees for clarity). x, y coordinates in arbitrary units.

(Top) Magnetic field lines (black); and approximate directions of ∇j_z (red arrows). (Bottom) Smoothed contours of vorticity (solid positive, dashed negative) superposed over shading for current intensity. $\mathbf{b} \cdot \nabla j_z$ matches the signs of locally generated vorticity.

quadrupoles (second column, first row) forming near each current sheet, precisely as expected from the above reasoning. The second row shows small portion of a much less orderly turbulence-style initial condition, from a hybrid PIC run. Here one sees many current sheets and filaments, highly distorted, and also a complex pattern of vorticity. Although in this case it is difficult to recognize the pattern of vorticity generation, we will see below that correlation statistics account for an interpretation very similar to what is seen in the simpler Orszag-Tang case.

V. VORTICITY AND EXPECTED KINETIC EFFECTS

Vortex quadrupoles form in kinetic plasma very much in the same way that they form in MHD, on the flanks of current sheets. Therefore one may also expect distinctive kinetic features to appear, such as ‘viscous like’ heating and thermal energy transport, given that the sharpest current sheets often form with a thickness a few times the ion inertial scale d_i . The basic mechanism for generating these kinetic effects can be thought of as a nonlinear generalization of Landau resonance, as one may understand based on a simple physical argument.

Protons gyrate in a left-handed sense about a uniform magnetic field. Fluid elements, defined here as parcels of

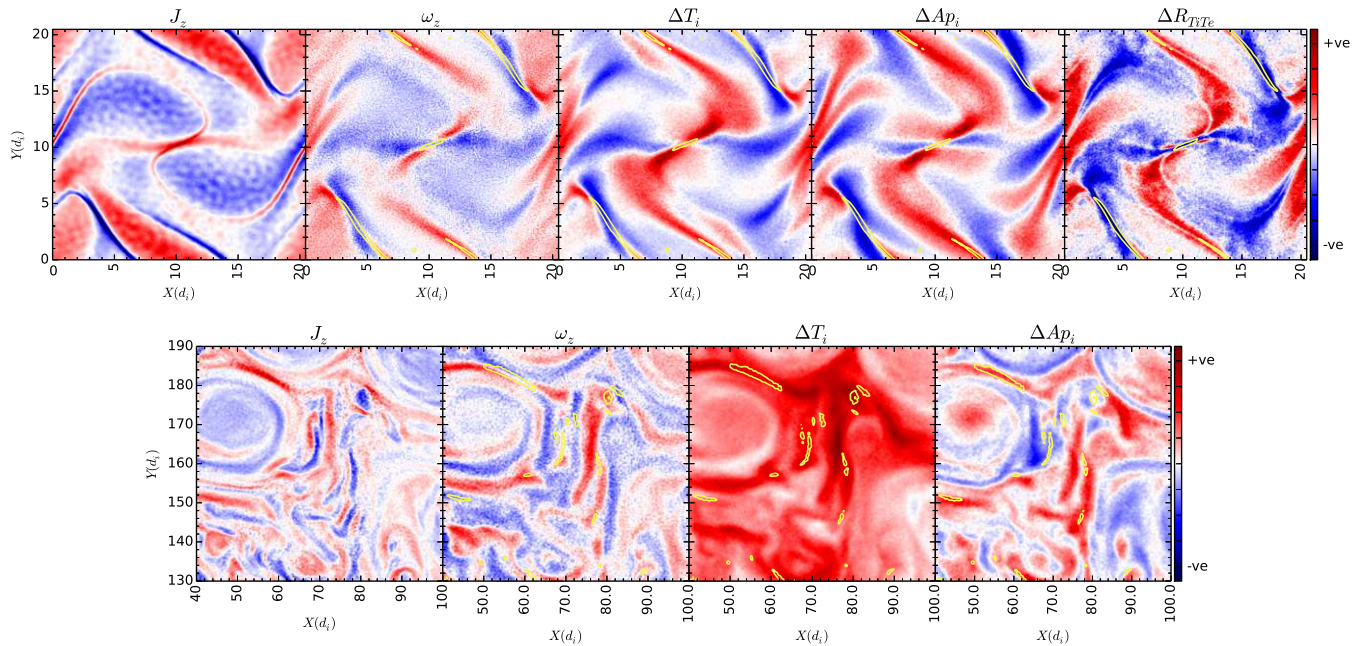


FIG. 2: Intermittency, or concentration into coherent structures of various quantities, from kinetic simulations. (Top) Orszag Tang PIC run, an orderly configuration in which structures and their relationships are relatively easy to identify at early times; (Left to right:) current density J_z ; out of plane vorticity ω_z proton temperature increase ΔT_i ; change in proton temperature anisotropy $\Delta A p_i$, and a measure of relative proton and electron heating. (Bottom) small portion of a hybrid turbulence run, in which structures are more complex and require statistical analysis. (Left to right: J_z , ω_j , ΔT_i , and $\Delta A p_i$. The notation $+ve$ and $-ve$ is shorthand for positive and negative, respectively.)

plasma following bulk motion as defined by the first moment of the distribution function, rotate in a right handed sense relative to the local vorticity vector ω . Therefore in locations where $\omega \cdot \mathbf{B}_0$ is positive, the protons gyrate opposite to the vortical motion of the fluid element. In a low collisionality or collisionless plasma, individual particles are not tightly coupled to fluid elements as they are in collisional gas dynamics, so under varying circumstances, protons may change fluid elements more or less rapidly. Clearly when the senses of rotation of particle and fluid element are mismatched, the protons have a higher probability of jumping from one fluid element to another one. A given fluid element will lose particles rapidly, but also gain particles that originate in elements that have different average velocities. Regionally there will be an exchange and interchange of fluid energy and random thermal energy. Intuitively this results either in an enhancement of heat transport, or an increase of thermal energy, or both.

The opposite happens in locations where $\omega \cdot \mathbf{B}_0$ is negative and hence the vortical motion of the fluid element and the proton gyration match. In this case the proton distribution has a higher probability of losing energy. This can be understood in a simple way. For definiteness suppose that plasma beta is unity and a current sheet of a few d_i thickness generates a (circular) vortex enhancement with similar dimension. Then particles gyrating in

the same sense of the vortex will remain within the vortex provided that their thermal speed is not much larger than the Alfvén speed. But higher energy particles - those in the tail of the distribution - will rapidly scatter away as their gyro-orbits exceed the dimension of the vortex. Similarly cooler particles that scatter into the vortex will easily be picked up by the fluid due to the $E \times B$ drift effect. The next effect is that the fluid elements in a $\omega \cdot \mathbf{B}_0 < 0$ vortex should have cooler protons.

Indeed, previous studies have demonstrated that there is a viscous-like effect associated with shear [24, 25] or vorticity [23] including the dependence on the sign of $\omega \cdot \mathbf{B}_0$. A recent hybrid simulation study [26] confirms that there is an association of kinetic effects, including proton temperature and proton temperature anisotropy, with this signed quantity [26].

At this point it is useful to recall a well-known general relationship that exists between *global* increase of internal energy and velocity gradients. This can be obtained from the Vlasov equation in suitable (e.g., periodic) boundaries using elementary manipulations. Specifically, it is straightforward to show that the kinetic energy $nm|\mathbf{v}_{th}|^2$ associated with random motions of any one species (say, protons) obeys the equation [62]

$$\begin{aligned} \frac{d}{dt} \frac{\langle nm|\mathbf{v}_{th}|^2 \rangle}{2} &= \frac{d}{dt} \frac{m}{2} \int d^3x \int d^3v f(\mathbf{x}, \mathbf{v}, t) |\mathbf{v} - \mathbf{u}|^2 \\ &= \langle u_i \nabla_j \Pi_{ij} \rangle = -\langle \Pi_{ij} \nabla_i u_j \rangle, \end{aligned} \quad (3)$$

in terms of the particle velocity \mathbf{v} , the fluid velocity of this species \mathbf{u} , and the pressure tensor Π_{ij} . The angle brackets $\langle \dots \rangle$ denote a volume average. Since the pressure tensor is always symmetric in indices, the full contraction $\Pi_{ij} \nabla_i u_j$ involves contributions only from the symmetric part of $\nabla_i u_j$. In general one can write $\nabla_i u_j = C\delta_{ij} + \frac{1}{2}S_{ij} + \frac{1}{2}\sigma_{ij}$ where $C = \nabla \cdot \mathbf{u}$ represents the compressional part, $S_{ij} = \nabla_i u_j + \nabla_j u_i - 2C\delta_{ij}$ is the traceless symmetric stress tensor, and the antisymmetric stress is $\sigma_{ij} = \epsilon_{ijk}\omega_k$.

The several considerations described in the present section and the previous one, including the references, provide the basis for the next section, in which we further unravel the complex kinetic processes that occur near coherent structures in turbulence. We should remark at this point that our main effort here pertains to current and vortex structures, but reconnecting current sheets will typically also occur near in regions where one also finds shocks, compressions and various linear waves, e.g., in the reconnection exhausts. All these phenomena may occur at least roughly in the vicinity of a current sheet. The typical location of these secondary structures is within a few d_i s of a current sheet and hence practically the same location in a system that extends to many decades in d_i . In large systems (large Reynolds numbers) the sites of vorticity generation may be so small that they are difficult to identify and hardly distinguishable in location from their companion current sheets [e.g. 61].

VI. STATISTICS AND LOCATION OF KINETIC EFFECTS

The proton temperature effects of vorticity generated near current sheets are clearly demonstrated in the case of the orderly Orszag-Tang vortex, as was the presence of the vortex quadrupole itself. In the third column, top row of Figure 2, we see an illustration of the change in proton temperature from its initial value $\Delta T_i = T_i - T_i(t=0)$ for this case, with the analogous plot from the more complex turbulence run in the second row. In the Orszag-Tang case one clearly sees that positive vorticity lobes ($\omega \cdot \mathbf{B}_0 > 0$ of the central quadrupole) are hotter, while the corresponding negative lobes are cooler. The fourth panel on each row of the same figure shows differential proton anisotropy $\Delta A_{pi} = T_{i\perp}/T_{i\parallel} - 1$ for each case. We also observe that the perpendicular anisotropy is greater in the hotter $\omega > 0$ lobes while the cooler $\omega < 0$ lobes have parallel anisotropy (negative ΔA_p). It is of course tempting to associate this phenomenon with the vorticity, as discussed by Franci et al. [e.g. 26]. We will discuss a nuance of this interpretation further below.

An additional diagnostic in the Orszag Tang PIC run is the relative heating of protons and electrons, shown in the final panel, top row of Figure 2. Out of many possible ways to quantify relative proton electron heating, we choose to work with differential relative heating defined by $\Delta R_{TiTe} = (T_i T_{e0}) / (T_e T_{i0}) - 1$, where T_{i0} and T_{e0} are the initial proton and electron temperatures. ΔR_{TiTe} is positive where the percentage increase in proton temperature is more than percentage change in electron temperature and vice versa. In the last panel of top row in Figure 2 it is evident that the $\omega \cdot \mathbf{B}_0 > 0$ lobes, with hot, more anisotropic protons, also have a proton population heated more than the electron population. The cooler, $\omega \cdot \mathbf{B}_0 < 0$ lobes have more electron heating than proton heating. In fact, beginning at the central current sheet (near the X-point) and moving outward along the current sheet flanks, one sees first (at the center) hotter electrons, then a region with almost equal proton and electron heating (along the flanks), and finally (outside the flanks) regions of hotter protons. Clearly, the organization of the vorticity into a quadrupolar structure is closely related to the spatial organization of kinetic activity and heating near the current sheet. Turning to the more turbulent hybrid run (second row, Fig. 2), we see that the proton temperature increase and the proton temperature anisotropy have a very patchy behavior. In this case it is more efficacious to carry out a statistical analysis, as done by Franci et al. [26].

Therefore, for the turbulent cases, we examine the association of kinetic effects with $\omega \cdot \mathbf{B}_0$, by computing conditional probability distribution functions (PDFs). For example we may look at ΔA_p , ΔT_i and ΔR_{TiTe} , extracting separate distributions, from the PIC simulation data depending on selected ranges of the values of ω_z . These ranges are (i) $\omega < -\sigma_{\omega zi}$; (ii) $-\sigma_{\omega zi} < \omega < \sigma_{\omega zi}$; and finally (iii) $\omega > \sigma_{\omega zi}$ where $\sigma_{\omega zi}$ is the rms value of proton vorticity. The resulting distributions for the PIC run Turb812 are shown in Figure 3 where one sees immediately that the most probable values of ΔA_p , ΔT_i and ΔR_{TiTe} systematically change with the selected ranges of vorticity. Large positive ω_z gives enhanced likelihood of hotter protons, more anisotropic protons and protons hotter than electrons. For highly negative ω_z one finds colder protons, lower anisotropy (parallel dominated) and relatively hotter electrons. This indicates a clear correlation between higher and anisotropic proton heating with positive $\omega \cdot \mathbf{B}_0$, consistent with the findings derived from inspection of the Orszag Tang PIC results described above, and consistent with the findings of Franci et al. [26] based on hybrid simulation.

The PIC simulation has a relatively complete description of the physics but is necessarily of smaller system size (25.6 d_i) and therefore smaller effective Reynolds number. For a higher Reynolds number view of the physics in Fig. (3), we turn again to a hybrid run (204.8 d_i). Conditional distributions for our hybrid run are shown in Fig. 4. In this case (top to bottom), we plot the distribution of proton temperatures ΔT_i conditioned on ranges of vor-

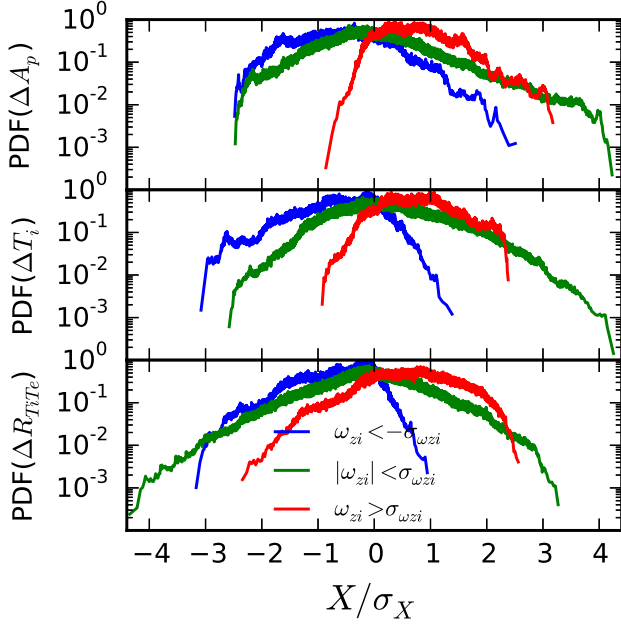


FIG. 3: Conditional PDFs for the PIC run: (top) ΔT_i (middle) ΔA_p ; and (bottom) T_p/T_e . In each case the pdfs are computed for three ranges of vorticity values: (i) $\omega < -\sigma$; (ii) $-\sigma < \omega < +\sigma$, and (iii) $\omega > \sigma$, where σ is the r.m.s. value of vorticity.

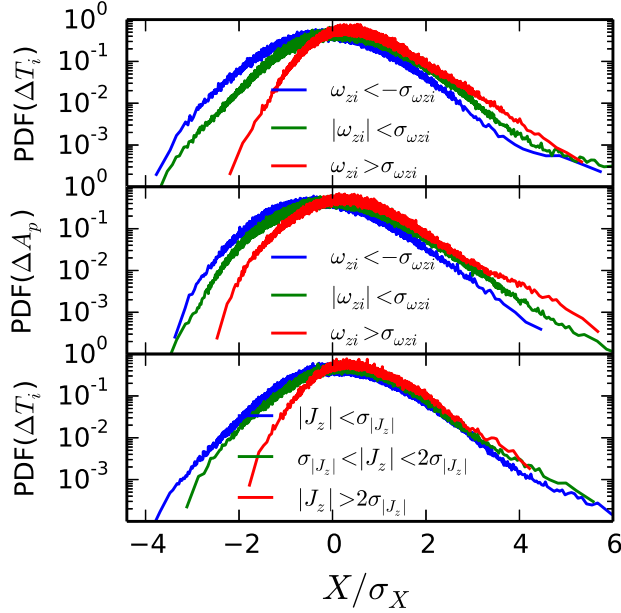


FIG. 4: Conditional PDFs for the hybrid run. (top) $pdf(T_i)$ conditioned on three ranges of vorticity; (middle) $pdf(\Delta A_p)$ conditioned on three ranges of vorticity; (bottom) $pdf(\Delta T_i)$ conditioned on three ranges of current density.

ticity, the distribution of proton temperature anisotropy conditions of ranges of vorticity, and the distribution of ΔT_i conditioned on ranges of the $|J_z|$. Here we find that proton heating is associated with both vorticity and current density but that the association with vorticity is the stronger of the two effects.

Having confirmed the expected statistical relations between vorticity and proton kinetic effects for the turbulent cases, it remains to quantify the spatial relationships between current sheets, vorticity concentrations, and kinetic effects. We accomplish this using two point correlations computed over the whole simulation domain. Figure 5 and Figure 6 show such correlations for the hybrid and PIC runs, respectively.

The top panel shows correlations between vorticity and current for the hybrid run. As current sheets are typically accompanied by vorticity generated in a quadrupole configuration, we find, on average, that the correlation between signed ω_z and J_z is close to zero for most part.

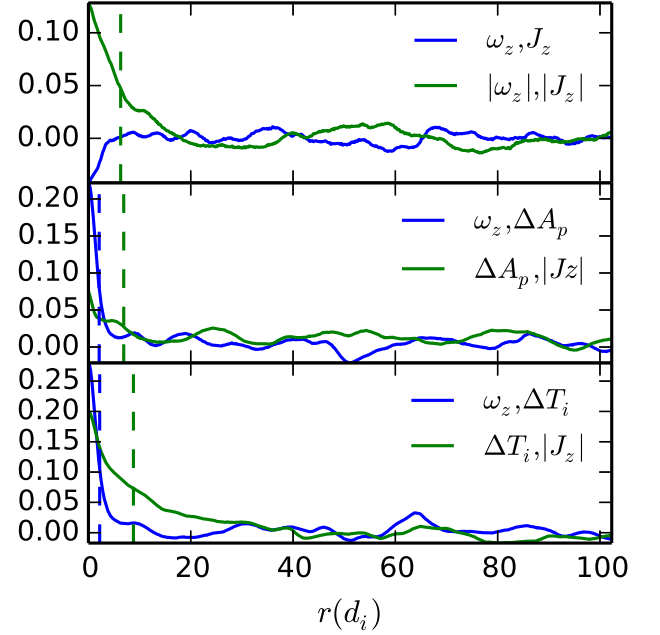


FIG. 5: Correlations between multiple quantities for the hybrid run.

In contrast, correlation curve for the *unsigned* ω_z and J_z clearly peaks at zero and drops to $1/e$ value in about $6d_i$ as shown by the vertical green dashed line in Fig. 5. This indicates the close juxtaposition of vorticity quadrupoles and current sheets. The numerical resolution in this simulation is $\Delta x = 0.1d_i = 0.5d_e$. Because of the coarse grid, the current sheets generally do not collapse to electron scales and hence the correlation between current sheets and vorticity goes to $\sim 6d_i$. The correlations for signed vorticity and ΔT_i drops in a few d_i s but the correlation of ΔT_i with current drops in about $6d_i$

like the correlation between vorticity and current. This is a direct quantification of the assertion that vorticity and kinetic effects, such as proton heating, occur “near” current sheets and that the vorticity structures are prime locations of energy exchange between fields and particles. The final panel of Fig. (5) shows the strong correlation between vorticity and proton anisotropy.

For completeness, we show similar correlations for the PIC run Turb812 in Figure 6. The correlations between vorticity and proton temperature as well as anisotropy drops to $1/e$ value in less than a d_i . This simulation had extremely fine grid scale, affording the possibility of collapse of current sheets to electron scales. Hence the correlations of proton heating and anisotropy to vorticity and current are much tighter than the hybrid run. The final panel of Figure 6 shows the correlation between current/vorticity and ΔR_{TiTe} which also peaks at zero and drops to $1/e$ value in less than a d_i . There is no clear correlation between ΔR_{TiTe} and current. This again is a direct quantification of the fact that protons are heated “near” current sheets and not exactly “in” current sheets [20, 54, 63].

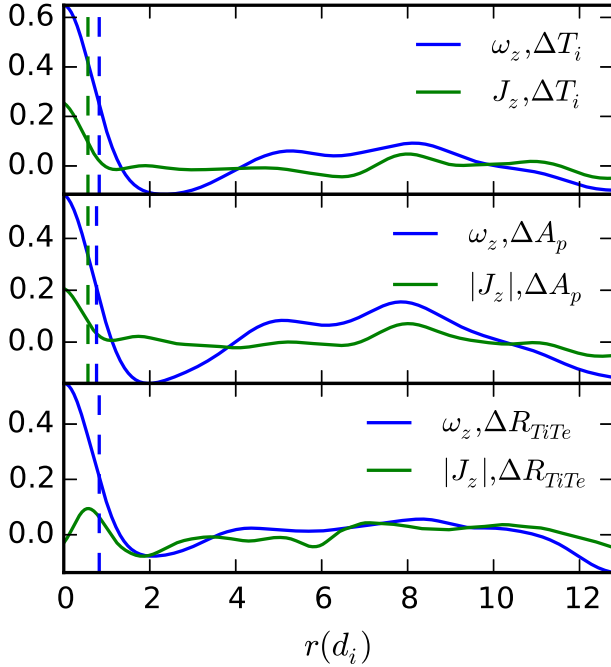


FIG. 6: Spatial correlations involving vorticity and current density, for PIC runs. (Top) proton temperature increase, correlated with current density and with vorticity, vs, spatial lag; (middle) vorticity and current correlations with proton temperature anisotropy; (bottom) Correlations with change in normalized proton to electron temperature ratio.

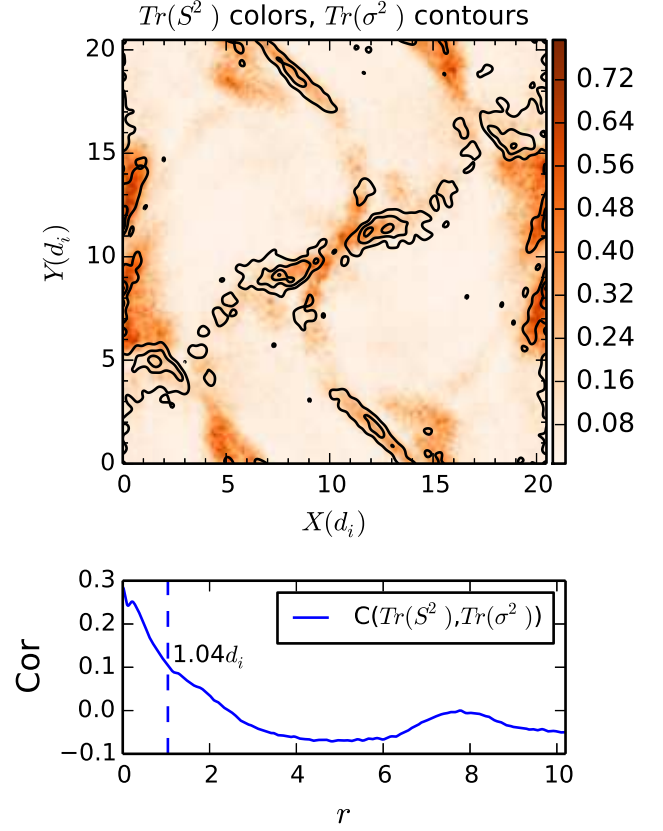


FIG. 7: Second invariants of the symmetric (S in color) and antisymmetric (σ black contours) stress tensors at initial time evolution of the PIC OTV simulation. The two can be seen to have strong proximity to each other. The proximity is further quantified by the two point correlation of these variables. It drops to $1/e$ value in about $1d_i$ as shown by the vertical dashed blue line.

VII. DISCUSSION

In this paper we have examined several ways in which vorticity enters into the dynamical activity near current sheets, thus contributing to an increasingly familiar scenario in which sharp gradients and coherent structures contribute to dissipation, kinetic effects including anisotropies, and heating.

The most studied cases of coherent structures in space plasmas have been current sheets or reconnection sites [44, 64, 65], at least in part due to the availability of magnetic field data from spacecraft with sufficient resolution to attain accurate detection at scales at or approaching kinetic scales. One would fully expect however that additional plasma variables such as velocity (and density, not shown here; however see Servidio et al. [22]) will be involved in intermittency and formation of coherent structures. In fact there have been numerous recent indications that velocity gradients might be responsible for

heating the plasma through a linear instability mechanism [24] or a viscous like interaction [45]. The conclusion that velocity gradients contribute to proton kinetic effects is supported by recent simulation Franci et al. [26], and based on solar wind observation [22]. Similar conclusions may be extended to sharp gradients in density as well as velocity and magnetic field.

In this context we may summarize our main conclusions, and suggest a broader context. Kinetic plasma turbulence forms current sheets, which like their MHD counterparts, generate vorticity nearby, in regions of strong current gradients. Various kinetic effects and heating of both protons and electrons take place in the vicinity of these current and vortex structures. We have shown here (see also Franci et al. [26]) that proton heating and anisotropy is better associated with vorticity rather than current, which provides some clarification to results that have shown [20, 21] that various kinetic effects are concentrated in the general vicinity of current sheets.

The idea that kinetic effects concentrate near current sheets in turbulence might easily extend to include effects such as flux pile-up, density compressions and particle trapping in secondary islands. All of these are likely features of the dynamics when current sheets form between interacting magnetic flux tubes. In this way, it may be useful to think of the general region within a few d_i neighborhood a strong current sheet as a kind of complex or generalized coherent structure involving juxtaposition of coherent structures in several variables – current, density, vorticity, compressions, heating to name a few. This agglomeration has been demonstrated to span a range of scales, e.g., from proton to electron inertial scales in the shear driven turbulent current sheets reported by Karimabadi et al. [41].

For large systems sizes and large effective Reynolds numbers it is likely that the dynamical interactions among several types of coherent structures become an important feature of the overall dynamics. In that case a fuller understanding of the complex dynamics within a “generalized coherent structure” becomes essential. Here we described a first step – a simple dynamical chain that leads from current sheet formation to vorticity quadrupole generation and emergence of enhanced proton kinetic effects.

One can actually see readily that even this situation must be more complex than we have described so far: From Eq. 3 we can deduce (see also [25]) that increase

of internal energy, or heating in the collisionless limit must be associated with the full contraction of the pressure tensor with the gradient tensor $\nabla_i u_j$. However, the pressure tensor is symmetric and gradient tensor may be written as a sum of symmetric strain and antisymmetric strain, the latter containing the vorticity. Therefore the only the symmetric stress and not the vorticity contributes directly to heating in the absence of collisions. So why do we see an association of vorticity and heating? For an empirical answer we refer to Fig 7 which shows the second invariant of the symmetric stress ($Det(S^2)$) and a measure of vorticity $Tr(\sigma^2)$ plotted in the simulation plane for the PIC OTV case at the same time as in Figure 2. Evidently there is a very high degree of correlation. The symmetric stress can produce heating, while vorticity can produce thermal anisotropy [23, 25]. Mathematically the two effects can be co-located even if they are formally independent because the current sheets are locally quasi-one-dimensional objects.

In this paper we have discussed the spatio-temporal relationship between current sheets, vorticity and kinetic processes such as proton heating, electron heating and anisotropy. As mentioned above, other quantities (e.g. density, compressions, localized linear waves, shock(lets), pressure dilations) also may be intermittent and may have strong correlations with current sheets. A detailed study of such processes is beyond the scope of this paper and will be discussed elsewhere. A detailed mathematical study of the relationship between symmetric and antisymmetric parts of the stress tensor is also beyond the scope of this study. An excellent start in that direction is the paper by Del Sarto et al. [25]. Further study will be needed to tighten the simple picture presented in this paper.

Acknowledgments

Research is supported by NSF AGS-1063439, AGS-1156094 (SHINE), AGS-1460130 (SHINE), and NASA grant NNX14AI63G (Heliophysics Grandchallenge Theory), the MMS mission through grant NNX14AC39G, and the Solar Probe Plus science team (ISIS/SWRI sub-contract No. D99031L). Some of the simulations were performed at the NCAR Yellowstone supercomputer.

-
- [1] A. Galeev, in *Physics of the Hot Plasma in the Magnetosphere*, edited by B. Hultqvist and L. Stenflo (Springer US, 1975), pp. 251–270, ISBN 978-1-4613-4439-1, URL http://dx.doi.org/10.1007/978-1-4613-4437-7_12.
 - [2] J. Saur, H. Politano, A. Pouquet, and W. H. Matthaeus, *Astronomy & Astrophysics* **386**, 699 (2002), URL <http://dx.doi.org/10.1051/0004-6361:20020305>.
 - [3] A. Retinò, D. Sundkvist, A. Vaivads, F. Mozer,

- M. André, and C. Owen, *Nature Physics* **3**, 236 (2007), ISSN 1745-2473.
- [4] T. Shimizu, *Publications of the Astronomical Society of Japan* **47**, 251 (1995).
- [5] C. Tu and E. Marsch, *Space Science Reviews* **73**, 1 (1995).
- [6] P. Sharma, G. W. Hammett, and E. Quataert, *The Astrophysical Journal* **596**, 1121 (2003).

- [7] C. L. Carilli and G. B. Taylor, Annual Review of Astronomy and Astrophysics **40**, 319 (2002), <http://dx.doi.org/10.1146/annurev.astro.40.060401.093852>, URL <http://dx.doi.org/10.1146/annurev.astro.40.060401.093852>.
- [8] P. J. Coleman, Jr., The Astrophysical Journal **153**, 371 (1968).
- [9] R. Bruno and V. Carbone, Living Reviews in Solar Physics **10** (2013), URL <http://www.livingreviews.org/lrsp-2013-2>.
- [10] E. Marsch, Living Reviews in Solar Physics **3** (2006), URL <http://www.livingreviews.org/lrsp-2006-1>.
- [11] M.-M. Mac Low, The Astrophysical Journal **524**, 169 (1999).
- [12] N. Banerjee and P. Sharma, Monthly Notices of the Royal Astronomical Society **443**, 687 (2014).
- [13] A. Barnes, The Astrophysical Journal **154**, 751 (1968).
- [14] A. Barnes, The Astrophysical Journal **155**, 311 (1969).
- [15] P. Hellinger, L. Matteini, Š. Štverák, P. Trávníček, and E. Marsch, Journal of Geophysical Research **116**, A09105 (2011).
- [16] P. Sharma, M. McCourt, E. Quataert, and I. J. Parrish, Monthly Notices of the Royal Astronomical Society **420**, 3174 (2012), URL <http://mnras.oxfordjournals.org/content/420/4/3174.full.pdf>, URL <http://mnras.oxfordjournals.org/content/420/4/3174.abstract>.
- [17] Y. L. Klimontovich, Physics-Uspexhi **40**, 21 (1997).
- [18] A. Schekochihin, S. Cowley, W. Dorland, G. Hammett, G. Howes, E. Quataert, and T. Tatsuno, The Astrophysical Journal Supplement Series **182**, 310 (2009).
- [19] G. Howes, Philosophical Transactions of the Royal Society of London A: Mathematical, Physical and Engineering Sciences **373**, 20140145 (2015).
- [20] S. Servidio, F. Valentini, F. Califano, and P. Veltri, Phys. Rev. Lett. **108**, 045001 (2012), URL <http://link.aps.org/doi/10.1103/PhysRevLett.108.045001>.
- [21] A. Greco, F. Valentini, S. Servidio, and W. Matthaeus, Physical Review E **86**, 066405 (2012).
- [22] S. Servidio, K. Osman, F. Valentini, D. Perrone, F. Califano, S. Chapman, W. Matthaeus, and P. Veltri, The Astrophysical Journal Letters **781**, L27 (2014).
- [23] J. Huba, Geophysical research letters **23**, 2907 (1996).
- [24] S. A. Markovskii, B. J. Vasquez, C. W. Smith, and J. V. Hollweg, The Astrophysical Journal **639**, 1177 (2006), <http://www.journals.uchicago.edu/doi/pdf/10.1086/499398>, URL <http://www.journals.uchicago.edu/doi/abs/10.1086/499398>.
- [25] D. Del Sarto, F. Pegoraro, and F. Califano, Physical Review E **93**, 053203 (2016).
- [26] L. Franci, P. Hellinger, L. Matteini, A. Verdini, and S. Landi, in *SOLAR WIND 14: Proceedings of the Fourteenth International Solar Wind Conference* (AIP Publishing, 2016), vol. 1720, p. 040003.
- [27] J. Hollweg and P. Isenberg, Journal of Geophysical Research **107**, 1147 (2002).
- [28] T. H. Stix, The Theory of Plasma Waves, New York: McGraw-Hill, 1962 **1** (1962).
- [29] T. N. Parashar, S. Servidio, M. A. Shay, W. H. Matthaeus, and P. A. Cassak, TWELFTH INTERNATIONAL SOLAR WIND CONFERENCE **1216**, 304 (2010), URL <http://link.aip.org/link/?APC/1216/304/1>.
- [30] T. Parashar, S. Servidio, M. Shay, B. Breech, and W. Matthaeus, Physics of Plasmas **18**, 092302 (2011).
- [31] K. T. Osman, W. H. Matthaeus, A. Greco, and S. Servidio, The Astrophysical Journal Letters **727**, L11 (2011), URL <http://stacks.iop.org/2041-8205/727/i=1/a=L11>.
- [32] M. Wan, W. Matthaeus, V. Roytershteyn, H. Karimabadi, T. Parashar, P. Wu, and M. Shay, Physical review letters **114**, 175002 (2015).
- [33] J. Chen and P. J. Palmadesso, Journal of Geophysical Research: Space Physics **91**, 1499 (1986).
- [34] B. D. G. Chandran, B. Li, B. N. Rogers, E. Quataert, and K. Germaschewski, The Astrophysical Journal **720**, 503 (2010), URL <http://stacks.iop.org/0004-637X/720/i=1/a=503>.
- [35] S. Bourouaine and B. D. Chandran, The Astrophysical Journal **774**, 96 (2013).
- [36] D. Sundkvist, A. Retinò, A. Vaivads, and S. D. Bale, Physical Review Letters **99**, 025004 (2007).
- [37] K. T. Osman, W. H. Matthaeus, B. Hnat, and S. C. Chapman, Phys. Rev. Lett. **108**, 261103 (2012), URL <http://link.aps.org/doi/10.1103/PhysRevLett.108.261103>.
- [38] P. Wu, S. Perri, K. Osman, M. Wan, W. Matthaeus, M. Shay, M. Goldstein, H. Karimabadi, and S. Chapman, The Astrophysical Journal Letters **763**, L30 (2013).
- [39] J. TenBarge and G. Howes, The Astrophysical Journal Letters **771**, L27 (2013).
- [40] M. Wan, W. Matthaeus, H. Karimabadi, V. Roytershteyn, M. Shay, P. Wu, W. Daughton, B. Loring, and S. Chapman, Physical Review Letters **109**, 195001 (2012).
- [41] H. Karimabadi, V. Roytershteyn, M. Wan, W. H. Matthaeus, W. Daughton, P. Wu, M. Shay, B. Loring, J. Borovsky, E. Leonardis, et al., Physics of Plasmas **20**, 012303 (2013), URL <http://scitation.aip.org/content/aip/journal/pop/20/1/10.1063/1.479392>.
- [42] V. Zhdankin, S. Boldyrev, J. Mason, and J. C. Perez, Physical review letters **108**, 175004 (2012).
- [43] K. Makwana, V. Zhdankin, H. Li, W. Daughton, and F. Cattaneo, Physics of Plasmas (1994-present) **22**, 042902 (2015).
- [44] A. Greco, P. Chuychai, W. H. Matthaeus, S. Servidio, and P. Dmitruk, Geophysical Research Letters **35**, 19111 (2008).
- [45] B. Vasquez and S. Markovskii, The Astrophysical Journal **747**, 19 (2012).
- [46] W. H. Matthaeus, Geophysical Research Letters **9**, 660 (1982).
- [47] J. F. Zeller, D. Biskamp, J. F. Drake, B. N. Rogers, M. A. Shay, and M. Scholer, J. Geophys. Res. **107**, 1230 (2002), doi:10.1029/2001JA000287.
- [48] P. Wu, M. Wan, W. Matthaeus, M. Shay, and M. Swisdak, Physical review letters **111**, 121105 (2013).
- [49] T. N. Parashar, S. Oughton, W. H. Matthaeus, and M. Wan, The Astrophysical Journal **824**, 44 (2016), URL <http://stacks.iop.org/0004-637X/824/i=1/a=44>.
- [50] S. Orszag and C. Tang, Journal of Fluid Mechanics **90**, 129 (1979).
- [51] R. Dahlburg and J. Picone, Physics of Fluids B: Plasma Physics **1**, 2153 (1989).
- [52] T. N. Parashar, M. A. Shay, P. A. Cassak, and W. H. Matthaeus, Physics of Plasmas **16**, 032310 (pages 7) (2009), URL <http://link.aip.org/link/?PHP/16/032310/1>.
- [53] T. N. Parashar, W. H. Matthaeus, M. A. Shay, and M. Wan, The Astrophysical Journal **811**, 112 (2015), URL <http://stacks.iop.org/0004-637X/811/i=2/a=112>.

- [54] W. H. Matthaeus, T. N. Parashar, M. Wan, and P. Wu, The Astrophysical Journal Letters **827**, L7 (2016), URL <http://stacks.iop.org/2041-8205/827/i=1/a=L7>.
- [55] D. Fyfe and D. Montgomery, Journal of Plasma Physics **16**, 181 (1976).
- [56] V. Carbone and A. Pouquet, in *Turbulence in Space Plasmas* (Springer, 2009), pp. 71–128.
- [57] E. N. Parker, *Cosmical magnetic fields: Their origin and their activity* (1979).
- [58] J. B. Taylor, Physical Review Letters **33**, 1139 (1974).
- [59] W. H. Matthaeus and D. Montgomery, Annals of the New York Academy of Sciences **357**, 203 (1980).
- [60] D. Biskamp, *Magnetohydrodynamic turbulence* (Cambridge University Press, 2003).
- [61] M. Wan, A. F. Rappazzo, W. H. Matthaeus, S. Servidio, and S. Oughton, The Astrophysical Journal **797**, 63 (2014), URL <http://stacks.iop.org/0004-637X/797/i=1/a=63>.
- [62] A. Hasegawa and T. Sato, *Space Plasma Physics: 1 Stationary Processes*, vol. 16 (Springer Science & Business Media, 2013).
- [63] P. Dmitruk, W. H. Matthaeus, and N. Seenu, The Astrophysical Journal **617**, 667 (2004), <http://www.journals.uchicago.edu/doi/pdf/10.1086/425301>, URL <http://www.journals.uchicago.edu/doi/abs/10.1086/425301>.
- [64] L. Sorriso-Valvo, V. Carbone, P. Veltri, G. Consolini, and R. Bruno, Geophysical Research Letters **26**, 1801 (1999), physics/9903043.
- [65] K. T. Osman, K. H. Kiyani, S. C. Chapman, and B. Hnat, The Astrophysical Journal Letters **783**, L27 (2014), 1311.5938.